RSC Advances

PAPER

View Article Online
View Journal | View Issue

Cite this: *RSC Adv.*, 2020, **10**, 34381

Enhancing the stability of the Rh/ZnO catalyst by the growth of ZIF-8 for the hydroformylation of higher olefins†

Lele Chen,‡[a] Jinghao Tian,‡[a] Huaxing Song,[a] Zhaohua Gao,[a] Haisheng Wei, *[ab] Wenhua Wang[ab] and Wanzhong Ren[ab]

Received 27th July 2020
Accepted 1st September 2020

DOI: 10.1039/d0ra06515c

rsc.li/rsc-advances

Hydroformylation of olefins is one of the most important industrial processes for aldehyde production. Therein, the leaching of active metals for heterogeneous catalysts is an important issue in the hydroformylation reaction, particularly for higher olefins to produce higher alcohols. Here, different Rh/ZnO catalysts with diverse ZnO as a support were investigated and a home-made ZnO_{50} support was selected to prepare the Rh/ZnO_{50}@ZIF-8 core–shell structure catalyst, which was synthesized by the growth of ZIF-8 with ZnO_{50} as the sacrificed template to afford Zn source. Compared with the Rh/ZnO_{50} catalyst, the Rh/ZnO_{50}@ZIF-8 catalyst demonstrated a better cyclic stability in the hydroformylation of 1-dodecene. Combining the experiment and characterization results, it was concluded that the ZIF-8 shell on the Rh/ZnO_{50} catalyst effectively prevented the leaching of metal Rh into the reaction solution. Moreover, the Rh/ZnO_{50}@ZIF-8 catalyst exhibited good universality for other higher olefins. This work provides a useful guideline for immobilizing the active species in heterogeneous catalysts for the hydroformylation reaction.

Introduction

The corresponding product aldehydes derived from the hydroformylation of olefins have wide applications, which include use as intermediates for alcohols, carboxylic acids, and aliphatic amines.[1–4] As for hydroformylation, numerous studies have been devoted to Rh-base catalysts, including homogeneous and heterogeneous catalysts.[5–10] In general, homogeneous catalysts with specific and uniform active sites possess high activity and selectivity but suffer from the problem of catalyst separation.[11,12] Therefore, two-phase systems have been exploited to solve the separation problem.[13–17] The noted RCH/RP biphasic system has been successfully applied in industries for the hydroformylation of propene; however, failure in the hydroformylation of higher olefins is due to their low solubility of substrates in water. In contrary, segregative heterogeneous catalysts with preferable industrial applications attract considerable attention.[18–20] However, there is a widespread concern over the issue that the active component of the Rh-base heterogeneous catalyst is easy to leach into the reaction solution as soluble Rh-carbonyl catalytically active species, which results in its low stability.[21] So, how to fix the active component in the hydroformylation catalyst is an important question to be solved. Much efforts focus on heterogenization of homogeneous catalysts by attaching phosphite ligands to a modified support.[22,23] Recently, it was found that a single Rh atom catalyst, which was formed by replacing the surface atom with the Rh atom[18,20] or dispersed Rh on N-doped carbon,[24] exhibited excellent performance.

Metal–organic frameworks (MOFs) have attracted considerable attention in confining nanoentities,[25] such as metal nanoparticles, clusters, single atom, biomacromolecules, to form composite materials,[26–31] which exhibited superior performance in numerous applications. Aiming at the loss of metal Rh in the hydroformylation reaction, MOF materials with high surface area and tunable pore size can serve as barriers to prevent the leaching of Rh species. Therein, zeolitic imidazolate framework-8 (ZIF-8), an important subgroup of MOFs with a pore size of 11.6 Å through 3.4 Å apertures, is taken into our consideration since it can be synthesized by growth on the ZnO surface to form a core–shell structure,[32,33] which is beneficial to confine the active metal under the shell material by a rational design. Owing to the small aperture of ZIF-8 materials, the loss of soluble Rh-carbonyl active species in the hydroformylation reaction will be hindered.

Herein, the Rh/ZnO@ZIF-8 catalyst was prepared using ZnO as the sacrificed template, and its catalytic performance was investigated in the hydroformylation of higher olefins. The

[a]*College of Chemistry and Chemical Engineering, Yantai University, Yantai 264005, Shandong, China. E-mail: haishengwei@ytu.edu.cn*

[b]*Collaborative Innovation Center of Comprehensive Utilization of Light Hydrocarbon Resource, Yantai University, Yantai 264005, Shandong, China*

† Electronic supplementary information (ESI) available. See DOI: 10.1039/d0ra06515c

‡ Lele Chen and Jinghao Tian have contributed equally to this work.

characterization and experiment results showed that the growth of a ZIF-8 shell on Rh/ZnO could effectively decrease the leaching of Rh and improve the stability of the catalyst.

Experimental section

Materials

Zinc nitrate hexahydrate ($Zn(NO_3)_2 \cdot 6H_2O$), 2-methylimidazole, ammonium carbonate, diethylene glycol, higher olefins, and ZnO nanoparticles were purchased from Aladdin Chemical Co., Ltd. (Shanghai, China) with analytical grade. Also, the commercial ZnO was denoted as ZnO-C. Rhodium chloride hydrate was purchased from Macklin. All the chemicals were used without further purification.

Synthesis of ZnO_{50} and ZnO-S

ZnO_{50} nanoparticles were prepared *via* the co-precipitation method. First, ammonium carbonate (4.0 g) was dissolved in 60 ml distilled water. Then, a 20 ml zinc nitrate solution (1 mol l^{-1}) was added dropwise to the ammonium carbonate solution at 50 °C and stirred for 3 h. The white precipitate was collected *via* filtration and washed several times with deionized water. The as-prepared sample was dried under vacuum at 60 °C overnight, and then calcined at 400 °C for 3 h to obtain ZnO_{50} nanoparticles. The ZnO sphere was prepared according to the previous literature[34] and denoted as ZnO-S.

Synthesis of Rh/ZnO@ZIF-8

Home-made ZnO_{50}, ZnO-C (commercial ZnO), and ZnO-S were selected as supports to impregnate using an $RhCl_3$ solution and dried at 60 °C to afford the 0.5% Rh/ZnO precursor. The Rh/ZnO_{50}@ZIF-8 catalyst was synthesized using the 0.5% Rh/ZnO_{50} precursor. Typically, 0.5% of theRh/ZnO_{50} precursor was put into a solution of 2-methylimidazole with ethanol as the solvent. The mixture was placed at room temperature without stirring for 3 h. Subsequently, the product was collected *via* centrifugation at 8000 rpm for 5 min, washed three times with ethanol, and then dried at 60 °C overnight.

Catalyst characterization

The X-ray diffraction (XRD) patterns were recorded from 5° to 80° at a scanning rate of 10° min^{-1} using a Rigaku Smart Lab III diffractometer using Cu Kα radiation (λ = 1.5406 Å). The morphology of samples was observed under a Hitachi S-4800 cold-cathode field-emission scanning electron microscope (FE-SEM). Fourier-transform infrared (FT-IR) spectroscopic characterization was performed on a Nicolet 380 instrument with a resolution of 4 cm^{-1}. The concentration of metal species was determined *via* inductively coupled plasma spectrometry-atomic emission spectrometry (ICP-AES) on an IRIS Intrepid II XSP instrument (Thermo Electron Corporation).

Catalytic test

Before the test, the catalysts were reduced under a H_2 atmosphere at 250 °C for 30 min. The catalytic performance of catalysts was evaluated in the hydroformylation of 1-dodecene using 1-octanol as an internal standard. In each experiment, 0.10 g of the catalyst and reaction solution were put into an autoclave and flushed with 10 bar CO/H_2 (1 : 1) for five times. Then, the autoclave was charged with CO/H_2 (1 : 1) until 4 MPa and heated to 90 °C in an oil bath with a magnetic stirrer to initiate the reaction. When the reaction completed, the catalyst was separated from the solution, and the product was analyzed using an Agilent 7890B gas chromatograph equipped with an HP-5 column.

Results and discussion

In order to obtain the Rh/ZnO@ZIF-8 catalyst with good catalytic performance, the precursor Rh/ZnO catalyst primarily has relatively better stability. Therefore, three types of Rh/ZnO catalysts with different morphologies of ZnO as supports were investigated. As shown in Fig. 1A–C, it can be seen that the home-made ZnO_{50} was small nanoparticles with an average size of about 20 nm. The other two ZnO supports in Fig. 1B and C were obviously larger than ZnO_{50} and exhibited rod-like and spherule shapes, corresponding to ZnO-C and ZnO-S. Fig. 1D shows the XRD pattern of different ZnO supports, and the diffraction peak of ZnO_{50} is weaker than that of other ZnO supports, which was in accordance with the SEM result. With different ZnO supports, 0.5% Rh/ZnO catalysts were prepared *via* incipient wetness impregnation. Also, the catalytic performance was tested in the hydroformylation of 1-dodecene. The results in Table 1 showed that the 0.5% Rh/ZnO-C catalyst exhibited the best catalytic performance with 96.7% conversion and 96.8% selectivity towards tridecylic aldehyde. For the 0.5% Rh/ZnO-S catalyst, it achieved 86.8% selectivity at the conversion of 98.9%. Over the 0.5% Rh/ZnO_{50} catalyst, the activity was lower than the preceding catalyst, the selectivity of aldehyde decreased to 79.3% under the same reaction conditions, which yielded more iso-alkenes. In addition, different catalysts showed a similar ratio of linear to the branched aldehyde in the products.

Further, the cyclic stability of numerous Rh/ZnO catalysts was conducted. The results in Fig. 2 show that the conversion and selectivity of three catalysts declined obviously in the second run. Comparatively speaking, 0.5% Rh/ZnO_{50} exhibited better stability, which maintained 65.2% conversion and 52.4% selectivity. In order to explore the deactivated reason, hot filter experiments were carried out. As shown in Table S1,† the filtration solution continued to react and achieved a higher conversion, revealing that soluble Rh active species were present in the filtration solution, which was confirmed by detecting the content of Rh in the filtration with ICP-AES. The results in Table S2† exhibit that the leaching of metal Rh from the 0.5% Rh/ZnO_{50} catalyst after the hydroformylation reaction was lower than that of the other two catalysts, which may be attributed to the ZnO_{50} support with small sizes and high surface areas. This also explained the better cyclic stability of the 0.5% Rh/ZnO_{50} catalyst. Meanwhile, according to the ICP results, the higher activity for 0.5% Rh/ZnO-C and 0.5% Rh/ZnO-S catalysts in Table 1 may be due to that the presence of

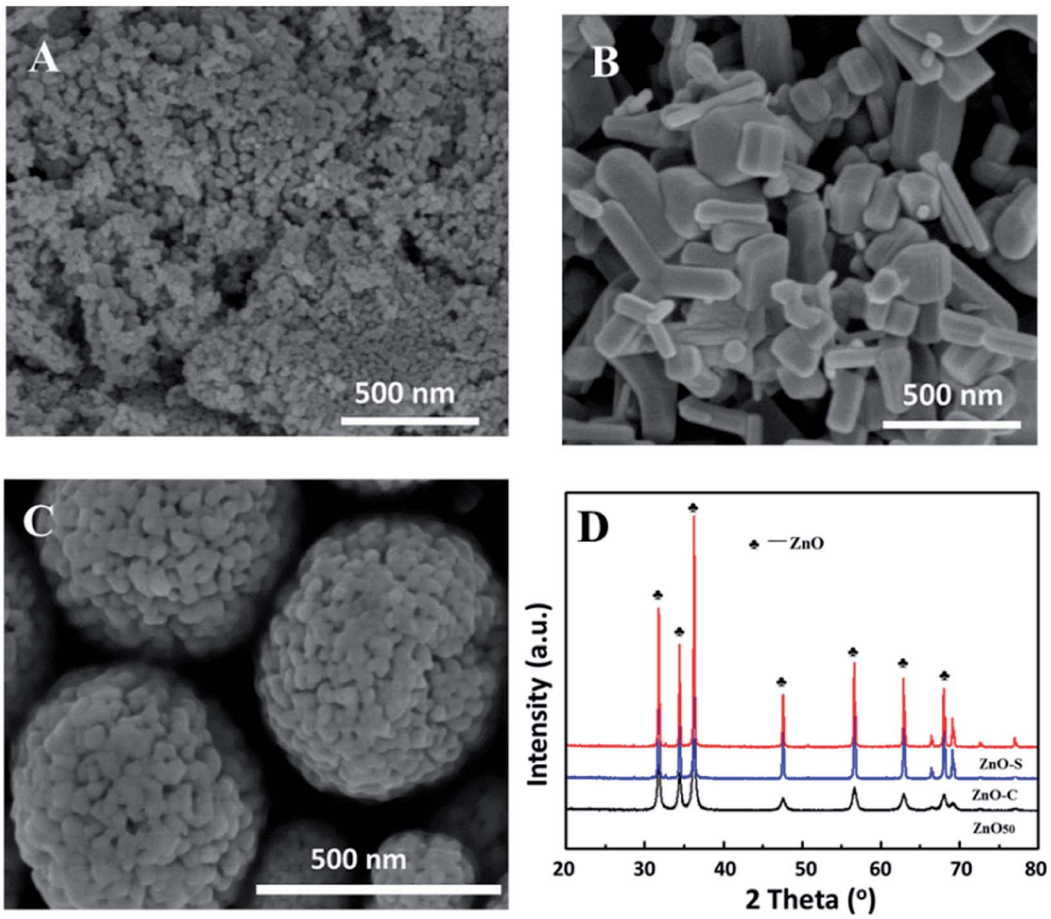

Fig. 1 SEM images of (A) ZnO_{50}, (B) ZnO-C, (C) ZnO-S, (D) XRD image of different ZnO.

Table 1 Hydroformylation results of 1-dodecene over different catalysts[a]

Catalyst	Conv. (%)	Aldehyde sel. (%)	Iso-alkene sel. (%)	L/B ratio
0.5% Rh/ZnO-C	96.7	96.8	3.2	0.7
0.5% Rh/ZnO-S	98.9	86.8	13.2	1.0
0.5% Rh/ZnO_{50}	92.4	79.3	21.7	1.2
0.5% Rh/ZnO_{50}@ZIF-8[b]	99.1	71.0	29.0	1.1

[a] Reaction condition: 4.0 MPa ($CO/H_2 = 1$), 90 °C, 2.5 mmol 1-dodecene, 1.0 mmol 1-octanol as internal standard, 2 h, L/B ratio refer to the ratio of linear to branched aldehyde in the products. [b] 4.5 h.

more homogeneous Rh active species in the solution, which also explained why the activity of different Rh/ZnO catalysts clearly declined after one cycle. So, in order to acquire a stable catalyst, the 0.5% Rh/ZnO_{50} catalyst was selected as the precursor to grow a ZIF-8 shell to avoid the loss of metal Rh.

First, the concentration of the 2-methylimidazole ligand was studied using ethanol as the solvent. In particular, the 0.5% Rh/ZnO_{50} precursor was put into the 2-methylimidazole solution with the concentration of 0.004, 0.02, 0.03 and 0.04 (g 2-methylimidazole/ml ethanol) for 3 h without stirring. Fig. 3A shows the XRD pattern of the samples after the growth of ZIF-8. It can be seen that no ZIF-8 crystal phase was observed when the concentration was 0.004. Increasing the concentration to 0.02, there appeared characteristic diffraction peaks of ZIF-8 at the 2θ range of 5–20°. Moreover, the intensity of the diffraction peak enhanced along with the addition of the ligand concentration, which agreed with the previous reports.[35] Moreover, the diffraction peak of ZnO_{50} still existed, which indicated that the formation of the ZIF-8 shell only consumed a portion of the ZnO_{50} support. The Rh/ZnO_{50}@ZIF-8 catalyst with the ligand concentration of 0.02 was further characterized *via* SEM, FT-IR, and XPS. In Fig. 3B, it can be clearly seen that the ZIF-8 crystals grew around ZnO_{50} nanoparticles to form a core–shell structure. The presence of the ZIF-8 shell was also determined *via* FT-IR characterization, as shown in Fig. 3C, which gave rise to the Zn–N stretch mode at 421 cm^{-1}, and the stretching and plane bending of the imidazole ring at 1350–1500 cm^{-1} and 500–1350 cm^{-1}, respectively.[36,37] For ZnO_{50} and Rh/ZnO_{50}, there was no distinctive band for ZIF-8, showing the same spectrum. Further, the XPS characterization was conducted to analyze the Rh/ZnO_{50}@ZIF-8 catalyst. As shown in Fig. 3D, the characteristic peaks of the Rh species were very weak because XPS only detected the surface information, and the binding energy of N 1s and Zn 2p were assigned to ZIF-8 materials.[30] These results

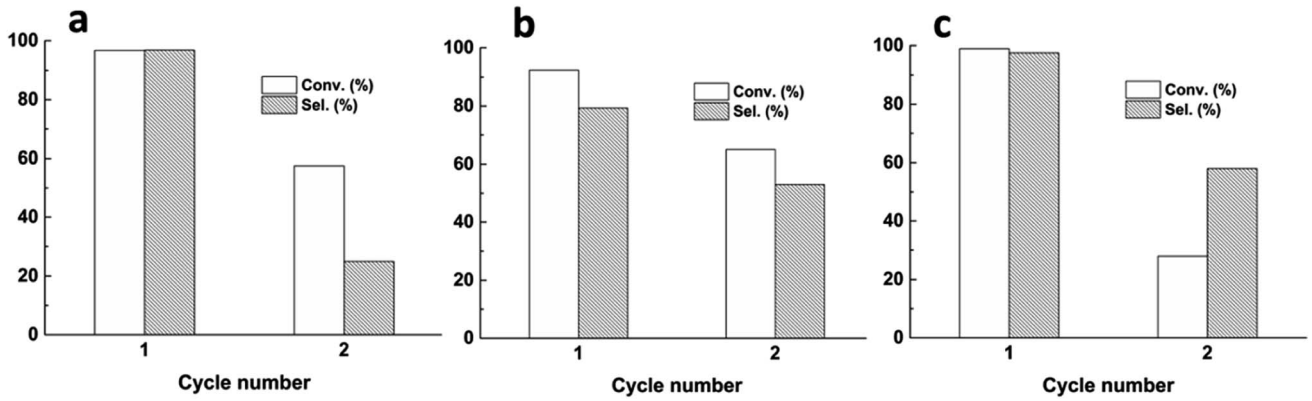

Fig. 2 Cyclic experiments of different catalysts, (a) Rh/ZnO-C, (b) Rh/ZnO_{50}, (c) Rh/ZnO-S.

confirmed that Rh/ZnO precursors were coated with ZIF-8 shells. In addition, it is well-known that ZIF-8 materials own high thermal stability, which starts to decompose at temperatures higher than 500 °C.[38] Here, the ZIF-8 crystal prepared with ZnO_{50} as a sacrificed template also maintained good stability under the N_2 atmosphere. As shown in Fig. S1,† the unique diffraction peak of ZIF-8 presented even at 500 °C, which was in accord with the TG result (Fig. S2†).

According to the above characterizations, the 0.5% Rh/ZnO_{50}@ZIF-8 catalyst prepared at the concentration of 2-methylimidazole at 0.02 was chosen to evaluate the cyclic stability. As shown in Table 1, the activity of the core–shell catalyst was obviously lower than that of the non-growth catalyst. For the 0.5% Rh/ZnO_{50}@ZIF-8 catalyst, it yielded 99.1% conversion and 71.0% selectivity towards the target product for 4.5 h. The decline in the activity may be attributed to the fact that the ZIF-8 shell inhibited the interactions between substrate and active species in the catalyst. The filtration solution was also detected, and the content of metal Rh decreased from 18.2% to 0.55% in Table S2,† indicating that the ZIF-8 shell effectively prevented the loss of metal Rh.[30] Moreover, the change in the conversion and selectivity for the Rh/ZnO_{50}@ZIF-8 catalyst was negligible after four cyclic experiments in Fig. 4, showing better stability compared with the Rh/ZnO_{50} catalyst,

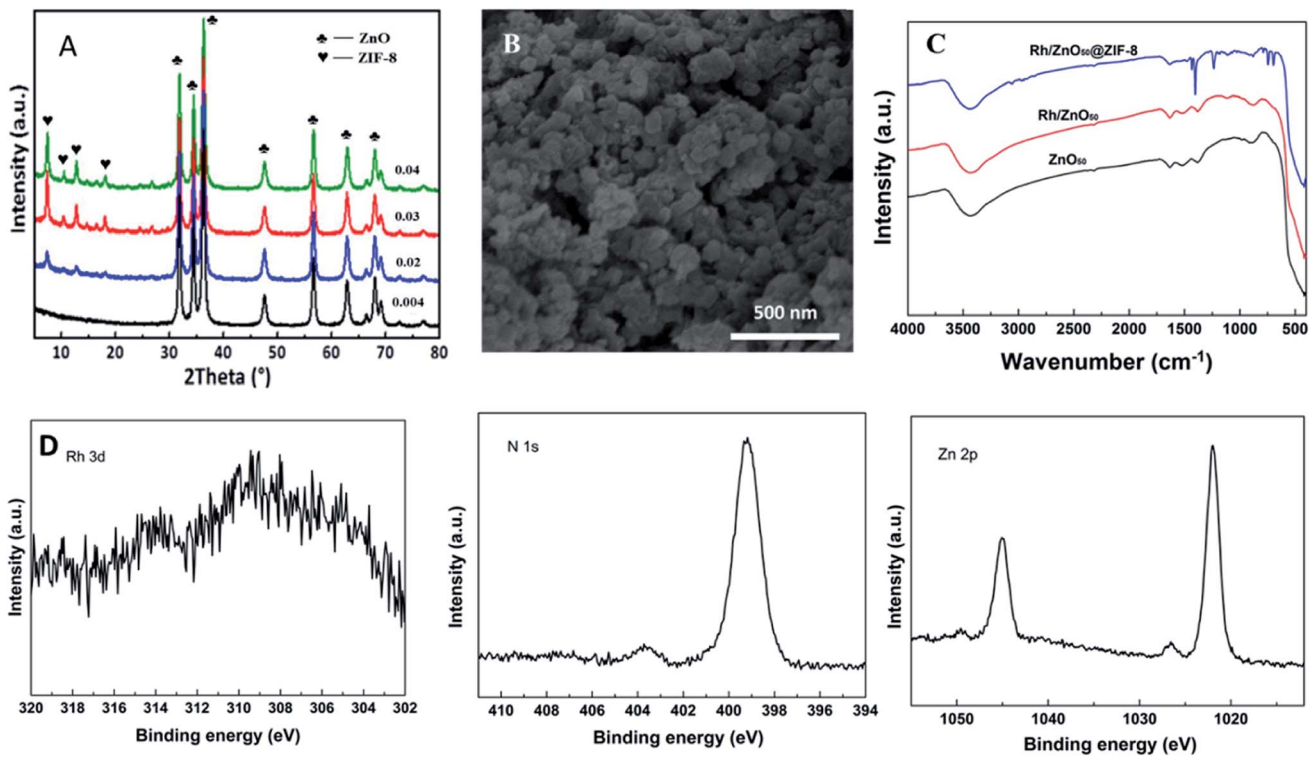

Fig. 3 (A) XRD pattern of 0.5% Rh/ZnO_{50}@ZIF-8 over different 2-methylimidazole concentrations, (B) SEM image of 0.5% Rh/ZnO_{50}@ZIF-8, (C) FT-IR spectra of numerous catalysts, (D) XPS spectra of 0.5% Rh/ZnO_{50}@ZIF-8 catalyst.

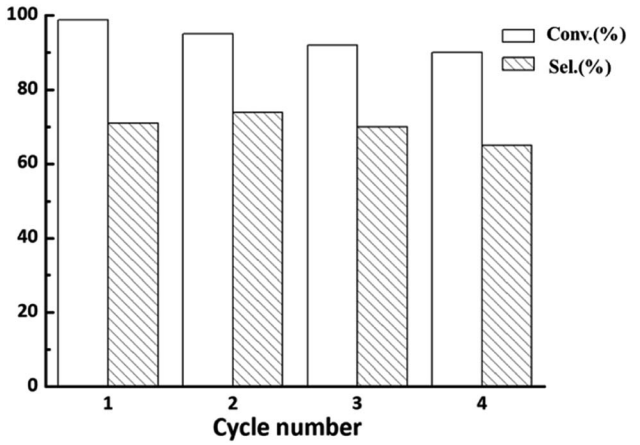

Fig. 4 Stability test for the 0.5% Rh/ZnO_{50}@ZIF-8 catalyst.

which was consistent with the previously reported works.[39,40] Moreover, the diffraction peak of the ZIF-8 structure in the Rh/ZnO_{50}@ZIF-8 catalyst remained invariable after the recycled test (Fig. S3†), exhibiting a good structure stability of ZIF-8 in the hydroformylation reaction condition. The work for further controlling the leaching of metal Rh is ongoing. In addition, the hydroformylation of other higher olefin substrates was also explored. As shown in Table S3,† the 0.5% Rh/ZnO_{50}@ZIF-8 catalyst revealed good catalytic performance in the hydroformylation of 1-hexene, 1-octene, and 1-decene, displaying excellent substrate universality.

Conclusion

The core–shell Rh/ZnO_{50}@ZIF-8 catalyst was synthesized by the growth of ZIF-8 on a home-made ZnO_{50} support, which was confirmed by SEM, XRD, and FT-IR characterizations. The catalytic performance was conducted in the hydroformylation of 1-dodecene, and the results showed that the Rh/ZnO_{50}@ZIF-8 catalyst exhibited better stability compared with the Rh/ZnO_{50} catalyst, which was due to the present of the ZIF-8 shell inhibiting the leaching of the Rh species.

Conflicts of interest

The authors declare that they have no conflict of interest.

Acknowledgements

This work has been supported from the National Natural Science Foundation of China, grant number: 21808193.

References

1 R. Franke, D. Selent and A. Borner, *Chem. Rev.*, 2012, **112**, 5675–5732.
2 M. Haumann and A. Riisager, *Chem. Rev.*, 2008, **108**, 1474–1497.
3 M. J. Climent, A. Corma and S. Iborra, *Chem. Rev.*, 2010, **111**, 1072–1133.
4 X. M. Zhang, S. M. Lu, M. M. Zhong, Y. P. Zhao and Q. H. Yang, *Chin. J. Catal.*, 2015, **36**, 168–174.
5 M. Beller, B. Cornils, C. D. Frohning and C. W. Kohlpaintner, *J. Mol. Catal. A: Chem.*, 1995, **104**, 17–85.
6 S. H. Chikkali, J. I. Vlugt and J. N. H. Reek, *Coord. Chem. Rev.*, 2014, **262**, 1–15.
7 F. Doro, J. N. H. Reek and P. W. N. M. Leeuwen, *Organometallics*, 2010, **29**, 4440–4447.
8 S. H. Chikkali, R. Bellini, B. Bruin, J. I. Vlugt and J. N. H. Reek, *J. Am. Chem. Soc.*, 2012, **134**(15), 6607–6616.
9 Q. Sun, M. Jiang, Z. Shen, Y. Jin, S. Pan, L. Wang, X. Meng, W. Chen, Y. Ding, J. Li and F. Xiao, *Chem. Commun.*, 2014, **50**, 11844–11847.
10 C. Li, K. Sun, W. Wang, L. Yan, X. Sun, Y. Wang, K. Xiong, Z. Zhan, Z. Jiang and Y. Ding, *J. Catal.*, 2017, **353**, 123–132.
11 J. Alemán and S. Cabrera, *Chem. Soc. Rev.*, 2013, **42**, 774–793.
12 J. Magano and J. R. Dunetz, *Chem. Rev.*, 2011, **111**, 2177–2250.
13 S. L. Desset, S. W. Reader and D. J. Cole-Hamilton, *Green Chem.*, 2009, **11**, 630–637.
14 X. R. Xue, Y. Song, Y. C. Xu and Y. H. Wang, *New J. Chem.*, 2018, **42**, 6640–6643.
15 Y. Zhao, X. Zhang, J. Sanjeevia and Q. Yang, *J. Catal.*, 2016, **334**, 52–59.
16 K. Kunna, C. Müller, J. Loos and D. Vogt, *Angew. Chem., Int. Ed.*, 2006, **45**, 7289–7292.
17 L. Tao, M. M. Zhong, J. Chen, S. Jayakumar, L. N. Liu, H. Li and Q. H. Yang, *Green Chem.*, 2018, **20**, 188–196.
18 R. Lang, T. Li, D. Matsumura, S. Miao, Y. Ren, Y. Cui, Y. Tan, B. Qiao, L. Li, A. Wang, X. Wang and T. Zhang, *Angew. Chem., Int. Ed.*, 2016, **55**(52), 16054–16058.
19 Y. K. Shi, G. Ji, Q. Hu, Y. Lu, X. J. Hu, B. L. Zhu and W. P. Huang, *New J. Chem.*, 2020, **44**, 20–23.
20 L. Wang, W. Zhang, S. Wang, Z. Gao, Z. Luo, X. Wang, R. Zeng, A. Li, H. Li, M. Wang, X. Zheng, J. Zhu, W. Zhang, C. Ma, R. Si and J. Zeng, *Nat. Commun.*, 2016, **7**, 14036.
21 S. M. Mcclure, M. J. Lundwall and D. W. Goodman, *Proc. Natl. Acad. Sci. U. S. A.*, 2011, **108**, 931–936.
22 A. C. B. Neves, M. J. F. Calvete, T. M. Melo and M. Pereira, *Eur. J. Org. Chem.*, 2012, 6309–6320.
23 W. Zhou and D. He, *Catal. Lett.*, 2009, **127**, 437–443.
24 Y. Xiong, J. C. Dong, Z. Q. Huang, P. Y. Xin, W. X. Chen, Y. Wang, Z. Li, Z. Jin, W. Xing, Z. B. Zhuang, J. Y. Ye, X. Wei, R. Cao, L. Gu, S. G. Sun, L. Zhuang, X. Q. Chen, H. Yang, C. Chen, Q. Peng, C. R. Chang, D. S. Wang and Y. D. Li, *Nat. Nanotechnol.*, 2020, **15**, 390–397.
25 L. Chen, R. Luque and Y. Li, *Chem. Soc. Rev.*, 2017, **46**, 4614–4630.
26 L. Chen, R. Luque and Y. Li, *Dalton Trans.*, 2018, **47**, 3663–3668.
27 B. Li, J. Ma and P. Cheng, *Angew. Chem., Int. Ed.*, 2018, **57**, 6834–6837.
28 Y. Liu, Z. Liu, D. Huang, M. Cheng, G. Zeng, C. Lai, C. Zhang, C. Zhou, W. Wang, D. Jiang, H. Wang and B. Shao, *Coord. Chem. Rev.*, 2019, **388**, 63–78.

29 Y. Yue, A. J. Binder, R. Song, Y. Cui, J. Chen, D. K. Hensley and S. Dai, *Dalton Trans.*, 2014, **43**, 17893–17898.
30 P. Liu, S. Liu and S. W. Bian, *J. Mater. Sci.*, 2017, **52**, 12121–12130.
31 S. F. Ji, Y. J. Chen, S. Zhao, W. X. Chen, L. J. Shi, Y. Wang, J. C. Dong, Z. Li, F. W. Li, C. Chen, Q. Peng, J. Li, D. S. Wang and Y. D. Li, *Angew. Chem., Int. Ed.*, 2019, **58**, 4271–4275.
32 G. Zhan and H. C. Zeng, *Chem. Commun.*, 2017, **53**, 72–81.
33 Y. Sun, Q. Zhang, X. Xu, L. Zhang, Z. Wu, J. Guo and G. Lu, *Eur. J. Inorg. Chem.*, 2016, 3553–3558.
34 X. Wang, J. Liu, S. Leong, X. Lin, J. Wei, B. Kong, Y. Xu, Z. Low, J. Yao and H. Wang, *ACS Appl. Mater. Interfaces*, 2016, **8**, 9080–9087.
35 Y. F. Yue, Z. A. Qiao, X. F. Li, A. J. Binder, E. Formo, Z. Pan, C. Tian, Z. Bi and S. Dai, *Cryst. Growth Des.*, 2013, **13**(3), 1002–1005.
36 L. Lin, H. Liu and X. Zhang, *Chem. Eng. J.*, 2017, **328**, 124–132.
37 Y. Hu, H. Kazemian, S. Rohani, Y. N. Huang and Y. Song, *Chem. Commun.*, 2011, **47**, 12694–12696.
38 S. P. Kyo, N. Zheng, A. P. Côté, J. Y. Choi, R. Huang, F. J. Uribe-Romo, H. K. Chae, M. O'Keeffe and O. M. Yaghi, *Proc. Natl. Acad. Sci. U. S. A.*, 2006, **103**, 10186–10191.
39 Q. H. Yang, Q. Xu, S. H. Yu and H. L. Jiang, *Angew. Chem., Int. Ed.*, 2016, **55**, 3685–3689.
40 B. J. Xi, Y. C. Tan and H. C. Zeng, *Chem. Mater.*, 2016, **28**, 326–336.

